Analytica Chimica Acta 942 (2016) 146–154

Contents lists available at ScienceDirect

Analytica Chimica Acta

journal homepage: www.elsevier.com/locate/aca

Titanium dioxide nanoparticle coating of polymethacrylate-based chromatographic monoliths for phosphopetides enrichment

Urh Černigoj [a, *], Jernej Gašperšič [a], Andreas Fichtenbaum [b], Nika Lendero Krajnc [a], Jana Vidič [a], Goran Mitulović [b], Aleš Štrancar [a, c]

[a] BIA Separations d.o.o., Mirce 21, SI-5270 Ajdovščina, Slovenia
[b] Medical University of Vienna, Clinical Department of Laboratory Medicine, Waehringer Guertel 18-20, A-1090 Wien, Austria
[c] The Centre of Excellence for Biosensors, Instrumentation and Process Control – COBIK, Tovarniška 26, SI-5270 Ajdovščina, Slovenia

HIGHLIGHT

- Simple immobilisation of rutile TiO_2 nanoparticles onto polymethacrylate monolith.
- Stable and homogeneous monolayer of TiO_2 nanoparticles was proven.
- Application of MOAC in combination with chromatographic monolith.
- Chromatographic separation of phosphorylated peptides from nonphosporylated.
- Enrichment of phosphorylated peptides from digested model protein.

GRAPHICAL ABSTRACT

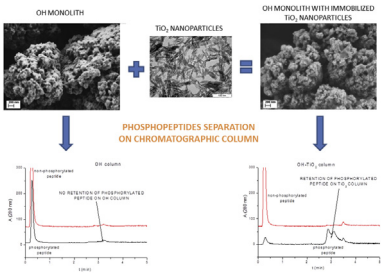

ARTICLE INFO

Article history:
Received 7 June 2016
Received in revised form
28 August 2016
Accepted 29 August 2016
Available online 19 September 2016

Keywords:
Proteomics
Monolith
Phosphopeptide enrichment
Chromatography

ABSTRACT

Metal oxide affinity chromatography has been one of the approaches for specific enrichment of phosphopeptides from complex samples, based on specific phosphopeptide adsorption forming bidentate chelates between phosphate anions and the surface of a metal oxide, such as TiO_2, ZrO_2, Fe_2O_3, and Al_2O_3. Due to convective mass transfer, flow-independent resolution and high dynamic binding capacity, monolith chromatographic supports have become important in studies where high resolution and selectivity are required. Here, we report the first synthesis and characterization of immobilisation of rutile TiO_2 nanoparticles onto organic monolithic chromatographic support (CIM-OH-TiO_2). We demonstrate the specificity of CIM-OH-TiO_2 column for enrichment of phosphopeptides by studying chromatographic separation of model phosphorylated and nonphosphorylated peptides as well as proving the phosphopeptide enrichment of digested bovine α-casein. The work described here opens the

Abbreviation: ACN, acetonitrile; ADHP, ammoniumdihydrogen phosphate; ATR, attenuated total reflection; BET, Brunauer–Emmett–Teller; BSA, bovine serum albumin; CID, collision induced dissociation; CIM, convective interaction media; CIM-OH, CIMac™ hydroxyl-based analytical column; CIM-OH-TiO_2, CIMac™ hydroxyl-based analytical column with immobilized TiO_2 nanoparticles; CV, column volume; DBC, dynamic binding capacity; ESI, electrospray ionization; FA, formic acid; FDR, false discovery rate; FTIR, Fourier transformation infrared spectroscopy; HPLC, high performance liquid chromatography; IMAC, immobilized metal affinity chromatography; LC, liquid chromatography; MeOH, methanol; mgf, mascot generic file; MPA, binding mobile phase – mobile phase A; MPB, elution buffer - mobile phase B; MOAC, metal oxide affinity chromatography; MS, mass spectrometry; MS/MS, tandem mass spectrometry; NaOH, sodium hydroxide; nPh, non-phosphopeptides; OH, hydroxyl group; Ph, phosphopeptides; RPLC, reverse phase chromatography; SEM, scanning electron microscopy; TEAB, triethylammonium bicarbonate; TEM, transmission electron microscopy; TFA, trifluoroacetic acid; TFE, trifluroethanol; XRD, x-ray diffraction.

* Corresponding author.
E-mail addresses: urh.cernigoj@monoliths.com (U. Černigoj), jernej.gaspersic@monoliths.com (J. Gašperšič), andreas.fichtenbaum@meduniwien.ac.at (A. Fichtenbaum), nika.lendero@gmail.com (N. Lendero Krajnc), jana.vidic@monoliths.com (J. Vidič), goran.mitulovic@meduniwien.ac.at (G. Mitulović), ales.strancar@monoliths.com (A. Štrancar).

http://dx.doi.org/10.1016/j.aca.2016.08.044

Metal oxide affinity chromatography
TiO_2 nanoparticles

possibility for a faster, more selective enrichment of phosphopeptides from biological samples that will enable future advances in studying protein phosphorylation.

1. Introduction

Protein phosphorylation is an essential ubiquitous post translational modification and plays important roles in regulation of vast array of cellular and molecular processes [1]. Due to the significance of protein phosphorylation in biological processes, many efforts have been made to investigate protein phosphorylation [2]. The complexity of phosphorylation (low stoichiometry, wide dynamic range, heterogeneity of phosphoprotein isoforms present in biological samples) requires highly sophisticated methods for in-depth investigations of protein phosphorylation, such as mass-spectrometry-based phosphoproteomics [3]. For biological significance, the latter requires high enrichment of phosphorylated molecules upstream of MS analyses [4]. The most common enrichment strategies are based on immobilized metal affinity chromatography (IMAC) and metal oxide affinity chromatography (MOAC). Due to its higher tolerance for low pH treatment of samples, required for protonation of carboxyl groups while keeping the negative charges on phosphorylated residues, MOAC leads to higher selectivity for phosphorylated molecules compared to IMAC [4]. Different metal oxides form complexes with phosphates in peptides and proteins, such as TiO_2, ZrO_2, Fe_2O_3, or Al_2O_3 [5–8]. If used in parallel, these MOAC materials have shown differences in affinity and specificity for phosphate groups and could therefore provide complementary information in phosphoproteome analysis [9]. Taking advantages of selectivity, recovery, and relatively high salt tolerance [10] TiO_2-based MOAC materials have been regarded as the most powerful and promising materials for phosphopeptide sample preparation [11].

TiO_2 naturally appears in three different crystalline forms and can be prepared as nano-sized particles or macroscopic crystals [12]. The main industrial application area is using it as a pigment in white paints, plastics, paper, textiles, cosmetics and food. Besides its use as a white pigment, TiO_2 has been studied for applications in photocatalysis [13], and nanocoating with different applications, such as super-hydrophilic surfaces and anti-reflective coatings [14]. Moreover, due to its inertness and high biocompatibility [15], TiO_2 presents a very suitable support as a biochromatographic stationary phase. Its usefulness as a chromatographic support has thus far been limited by the challenges presented by introduction of chromatographically active ligands onto solid TiO_2 chromatographic supports. To date, organic molecules could only be immobilized onto titania surface by exploiting the strong chemical coordinative adsorption mechanism of carboxyl groups in dicarboxylic or tetracarboxylic molecules (binding constant $K \approx 10^4$–10^5 M^{-1} and 10^5–10^6 M^{-1}, respectively) [16,17]. A similar coordinative adsorption mechanism was proposed for phosphate groups ($K \approx 10^4$–10^5 M^{-1}) [18], which has been used to rationalise the affinity interaction between phosphorylated proteins and peptides and TiO_2 surface [19].

Traditionally, phosphoprotein enrichment has been achieved using macroscopic TiO_2 particles [8,11], though nano-sized TiO_2 would be advantageous due to higher contact area with phosphopeptides and phosphoproteins. This approach suffers from difficult handling, aggregation of particles and possible toxicity of nanoparticle [20–22]. An elegant solution combining the advantages of macroscopic and nano TiO_2 is to prepare a pure TiO_2 monolithic column from titanium precursors, but due to the complexity of such synthesis and problems with leaking there are just few successful reports of TiO_2 capillary monoliths [23]. We reasoned, therefore, that the immobilisation of nano-sized TiO_2 onto a surface of a macroporous chromatographic support would harness the benefits both of nano-particulate TiO_2 as ligands for selective phosphopeptide enrichment, and unique chromatographic properties of monolith supports, while minimising the issues with handling and toxicity of TiO_2. Polymethacrylate monolithic supports have been reported as innovative chromatographic matrices with high porosity and convective mass transport [24,25], therefore integration of nanoparticles onto such material appeared as an alternative solution [26]. Different types of nanoparticles (gold, iron oxides, latex, carbon nanotubes, and hydroxyapatite) have been integrated onto monolithic supports either via encapsulation during polymerization [27–29] or by immobilisation of nanoparticles (but not TiO_2) directly onto monolith pore surface [30,31]. The latter approach results in a significant increase in the effective surface area due to the high surface-to-volume ratio of nanomaterials. To our knowledge there are no existing reports in the literature, describing the immobilisation of TiO_2 nanoparticles onto monolithic support. TiO_2 reacts coordinatively with aromatic diol groups (bidentate mechanism), such as in catechol [32], strong interactions of aliphatic diols with TiO_2 surface (molecularly adsorbed) have also predicted [33], which have not yet been exploited to immobilize TiO_2 nanoparticles to a polymeric support. In this article we describe a successful coating of rutile TiO_2 nanoparticles onto hydroxyl-based (OH) Convective Interaction Media™ (CIM™) chromatographic support (CIM-OH-TiO_2 column). Composite material characterization data on CIM-OH-TiO_2 columns are evaluated and a selectivity of the column for model peptides is demonstrated.

2. Materials and methods

2.1. Materials

Pure rutile TiO_2 nanoparticles sol in aqueous system at pH 3.6 (40 mg mL^{-1}) were obtained from University of Debrecen, Hungary. Phosphorylated and nonphosporylated peptides were designed at the Medical University of Vienna and synthesized at University of Debrecen (Table 1). Raw phosphopeptides were purified using reversed phase chromatography on a PepMap C18 column (300 μm ID × 15 cm length, 100 Å pore size, 3 μm particle size, Thermo Scientific, Germering, Germany). Sodium hydroxide (NaOH, 98%), 96% H_2SO_4, acetic acid (AA, 99.8%), 37% HCl (99.8% purity), sodium chloride (NaCl, 99.8%), trisodium phosphate (99%), formic acid (FA, 98%), HPLC grade acetonitrile (ACN), triethylammonium bicarbonate (TEAB, 1 M, pH 8.5 ± 0.1), 2,5-dihydroxybenzoic acid (DHB, >99.0%) and proteins (ovalbumin, phosvitin, α-casein, cytochrome C, lysozyme and human serum albumin; all of them with purity higher than 95%) were purchased from Sigma-Aldrich (St. Louis, MO, USA); ammonium hydroxide, trifluoroacetic acid (TFA, 98%), heptaflurobutyric acid (HFBA, 99.5%), and sodium 1-octanesulfonate monohydrate (1-OSA,~98%) were purchased from Fluka (St. Gallen, Switzerland); disodium hydrogen phosphate (99%) was purchased from Honeywell (Morristown, NJ, USA). HPLC grade methanol (MeOH) and ammonium dihydrogen phosphate (ADHP, PhEur) were

Table 1
Sequences of the model peptides used for chromatographic separation - phosphorylation sites are marked with bold font.

Peptide	Phosporylation	Sequence
NP	Nonphosphorylated	WWGSGPSGSGGSGGGK
1P	One phosphorylated site	WWGSGPSGSGGSGGGK
2Pa	Two phosphorylated sites	WWGSGPSGSGGSGGGK
2Pb	Two phosphorylated sites	WWGSGPSGSGGSGGGK
3P	Three phosphorylated sites	WWGSGPSGSGGSGGGK
4P	Four phosporylated sites	WWGSGPSGSGGSGGGK

purchased from Merck Wien, Austria. HPLC grade water was prepared using a Milli-Q plus device from Millipore, Wien, Austria. Sequencing grade modified trypsin was purchased from Promega (Mannheim, Germany), and trifluoroethanol (TFE, ≥99.9%) from Alfa Aesar, Karlsruhe, Germany. All buffer solutions were filtered through a 0.22 μm PES membrane filter (TPP, Switzerland). Ethanol (96%) was purchased from Kefo (Ljubljana, Slovenia).

OH modified CIMac monolithic analytical columns (CIM-OH column) with dimensions of 5.2 mm in diameter (I.D.) x 5 mm in length (volume 0.106 mL) as well as micro analytical columns (micro-CIM-OH column) with dimensions of 1.0 mm in diameter (I.D.) × 5 mm in length (volume 0.004 mL) with pore size diameters of 2 μm were provided by BIA Separations (Ajdovščina, Slovenia).

2.2. Methods

2.2.1. CIM-OH-TiO_2 and micro-CIM-OH-TiO_2 column preparation

The initial TiO_2 sol (40 mg of TiO_2 mL^{-1}) was diluted to a final concentration of 1 mg mL^{-1} with 10 mM acetate + 0.5 M NaCl buffer, pH 3.9. CIM-OH columns were washed with 10 mM acetate +0.5 M NaCl buffer, pH 3.9, followed by the diluted TiO_2 sol at 0.5 mL min^{-1}. The turbidity of the suspension at the outlet was monitored by UV–Vis measurements at 600 nm and the TiO_2 loading was stopped when the turbidity of the sample reached the turbidity of the loading sample. The columns were washed with ddH_2O followed by curing of the composite. The columns were then washed with 20% ethanol (v/v) and aqueous mobile phase. The same procedure was applied for micro-CIM-OH-TiO_2 columns except the lower flow rate applied (0.05 mL min^{-1}).

When performing stability testing of the immobilized layer, columns were washed according to the following protocol: 10 column volumes (CV) water, followed by 30 CV of 1.0 M NaOH with additional soaking in 1.0 M NaOH for 15 min, then washing with ddH_2O until solution reached pH 7.0, followed by washing with 30 CV of 0.1 M HCl with additional soaking in 0.1 M HCl for 15 min, then washing with water until the solution reached pH 7.0.

2.2.2. Characterization of the CIM-OH-TiO_2 composite column

Pore size distribution was measured by a Pascal 440 (Thermo-Quest Italia, Rodano, Italy) mercury porosimeter within the range 15–10 000 nm. Approximately 0.1 g of dried monolith sample was measured.

FTIR (Fourier transformation infrared spectroscopy) spectra of dried TiO_2 starting material and of dried CIM-OH as well as of CIM-OH-TiO_2 monolith were recorded using attenuated total reflection (ATR) technique by a Nicolet iS5 instrument coupled with iD5 ATR accessory (Thermo Fisher Scientific, Waltham, MA, USA).

Nitrogen physisorption measurements were performed on a Tristar volumetric adsorption analyzer (Micromeritics). The Brunauer–Emmett–Teller (BET) specific surface area, S_{BET}, was calculated using the adsorption branch in the relative pressure range between 0.05 and 0.30.

Morphology of the monolithic matrix and the composite product was measured using scanning electron microscopy (SEM) on Zeiss Supra™ 3VP microscope.

The x-ray diffraction (XRD) patterns of dried TiO_2 and composite material were obtained on a XPert Pro PW3040/60 (Panalytical, Almelo, The Netherlands) using CuKa radiation (k = 1.5406 Å). Samples were scanned over a range of 20–60° 2θ with a step of 0.04°.

2.2.3. Chromatographic characterization of CIM-OH-TiO_2 columns

2.2.3.1. Testing of phosphoprotein and phosphopeptide binding onto CIM-OH-TiO_2 columns. Preliminary chromatographic studies were performed on Agilent (1200 series) or Knauer MicroHPLC system with Shimadzu SPD-20A detector. Flow rate was 1.0 mL min^{-1}, absorbance signal was measured at 280 nm and 215 nm. Tryptophan fluorescence was measured with excitation wavelength 280 nm and emission wavelength 340 nm. CIM-OH (negative control) and CIM-OH-TiO_2 analytical columns were evaluated for phosphoproteins and phosphopeptides separation and enrichment.

Different binding buffers for phosphoproteins were tested, such as 0.1% TFA (v/v) or 1% acetic acid (v/v), in both cases with or without the addition of 100 mM NaCl. 10 μl of 1 mg mL^{-1} of the sample was then injected onto the column. The dynamic binding capacity (DBC) for ovalbumin was measured with 1.0 mg mL^{-1} ovalbumin solution dissolved in 1% acetic acid + 100 mM NaCl. The phosphoproteins were eluted in 3 min long gradient to 50 mM (or 0.5 M) sodium phosphate pH 12 + 100 mM NaCl (mobile phase B - MPB). The optimized chromatographic conditions were used for phosphopeptides separation as well.

2.2.3.2. α-casein digestion and phosphopeptide enrichment. Phosphopeptide enrichment of tryptically digested bovine α-casein was performed using a micro-CIM-OH-TiO_2 column.

Sample loading and elution of bovine α-casein was carried out using an "Elite syringe pump" (Harvard Apparatus, Holliston, United States) with a glass syringe (Hamilton).

RPLC-MS peptide separation was conducted using a nano-LC system consisting of a Famos autosampler, "Switchos" column switching module and an "Ultimate" pumping and UV detection module (Thermo Scientific, Germering, Germany - former LC Packings, Amsterdam, The Netherlands). Sample loading and desalting of fractions prior to the nano HPLC separation was performed on a PepMap C18 trap-column (300 μmID × 5 mm length, 5 μm particle size, 100 Å pore size). The analytical column was a 75 μm ID × 25 cm length Acclaim® PepMap100 (C18, 3 μm particle size, 100 Å pore size). The mass spectrometric analysis was performed on an LTQ Velos ion-trap mass spectrometer (ThermoFisher

Table 2
Compositions of mobile phases used for phosphopeptide trapping on the micro-CIM-OH-TiO_2 monolithic supports.

Mobile phase	Short name	Solvent components	Purpose
Loading solvent	LS	20% acetic acid, 420 mM 1-OSA, 50 mg mL^{-1} dihydroxybenzoic acid, 0.1% heptaflurobutyric acid	Column equilibration, sample dilution and loading
Wash solvent 1	LS	same as "Loading solvent"	First column wash
Wash solvent 2	W2	80%acetonitrile, 0.1% trifluoroacetic acid	Second column wash
Elution solvent	ES	50% 50 mM ADHP, pH 10.5 adjusted with ammonia solution/50% acetonitrile	Phosphopeptide (Ph) elution

Scientific, Bremen, Germany) equipped with the Proxeon nano ESI source (Proxeon, Odense, Denmark), operated in positive nano electrospray (ESI) mode.

Bovine α - casein was weighed on a precision scale and dissolved using the digestion buffer (50 mM TEAB). Tryptic digest of α-casein was performed by direct addition of sequencing grade modified porcine trypsin (Promega, Mannheim, Germany) applying a 1/50 (w/w) ratio of trypsin/protein. The incubation time was 17 h at 37 °C. Mobile phases for phosphopeptide enrichment were prepared as described by Mazanek et al. [34,35] and following table enlists detailed information on applied mobile phases.

The phosphopeptide trapping experiment were repeated four times. Upon equilibration of the micro-CIM-OH-TiO_2 column, 2 μg of tryptically digested bovine α-casein was diluted in 40 μl loading solvent and loaded on the TiO_2 column using a flow of 3 μl min^{-1}. Fractions were collected according to the following table.

Subsequently, EL fraction was acidified by addition of 10 μl TFA for subsequent reversed phase separation and MS/MS analysis. For RPLC-MS-analysis, 2.5% of FT and EL fraction's original volume was injected. Therefore, fractions were diluted using 0.1% TFA and dilution ratio of 1/20 (FT) or 1/15 (EL) to a final volume of 40 μl, whereof 20 μl was loaded for RPLC-MS analysis. Table 3.

Additionally, 2 μg of the bovine α-casein digest was diluted in a ratio of 1/20 using loading solvent, in the same way as fraction "FT". This sample, named "Dig in LS", served as a control sample representing the extent of MS phosphopeptides identification rates under conditions without preceding phosphopeptide trapping.

2.2.3.3. Nano-RPLC-MS conditions. Three fractions - FT, EL and Dig in LS - from bovine α -casein were loaded onto a C18 trap column using 0.1% TFA as the loading mobile phase at a flow rate of 50 μl min^{-1} for 8 min. During the loading, buffer salts were removed and peptides were concentrated on the trap column. Separation gradient was conducted for 64 min as shown in Table 4.

Potential carryover of the HPLC system was reduced by treating the needle, the trap column, and analytical column with mobile phases containing trifluoroethanol, as described by Mitulović et al. [36].

The trap column was operated at ambient temperature (23 °C–25 °C) while the analytical column was mounted in a column oven at 60 °C and was operated at 300 nl min^{-1}. Peptides eluting from the analytical C18 column were detected using a UV detector, equipped with a nano flow cell (3 nl), at 214 nm and with the LTQ ion trap mass spectrometer operated in positive electrospray mode.

Mass spectrometer scanned the mass range from 300 to 1800 *m/z* using a top-fifteen data-dependent mode for MS/MS operations. Isolation width for parent ion scans was set to 2 *m/z* and CID fragmentation with 35% normalized collision energy for 10 ms and a Q value of 0.25, dynamic exclusion was set with 30 s at a repeat count of 1.

Raw files of acquired MS/MS data were converted into *mgf* peak lists using the MSconvert software (http://proteowizard.sourceforge.net/project.shtml).

For the MS/MS ion search peak lists from replicate fractions (n = 2 for each fraction) were merged and searched against the most recent SwissProt bovine database using an in-house Mascot 2.51 server (Matrix Science, London, UK). For database searches, phosphorylation on serine, tyrosine and threonine were selected as variable modifications. The precursor peptide mass and the MS/MS peptides mass tolerance were set to +/− 0.8 Da.

Mascot search results were adjusted by setting the ion - score cut-off to 20, and the resulting identification lists were subsequently exported into the CSV file format for further data analysis using Microsoft Excel 2010© and the database software FileMaker Pro 14© [37].

3. Results and discussion

3.1. Synthesis and characterization of CIM-OH-TiO_2 column

As discussed in the introduction, our attempt was to use monolithic support, functionalized with aliphatic diol group, for the immobilisation of TiO_2 nanoparticles. Commercially available CIM-OH monolith columns contain the diol functionality and were therefore used as a platform for immobilising TiO_2 nanoparticles as described in Materials and Methods.

Initially, immobilisation of TiO_2 crystals was attempted onto monoliths with average pore size diameter of 1.5 μm. TiO_2 sample was composed of TiO_2 needles, approximately 100 nm long and 20 nm wide (Fig. 2C). This approach led to irreversible clogging of the monolith macroporous channels with TiO_2 needless. Since the pH of the diluted TiO_2 aqueous solution (pH 3.9) was close to the isoelectric point of TiO_2 (pH between 6 and 7), it was speculated that the particles aggregated within the monolith channels, leading

Table 3
Mobile phases and chromatographic conditions for phosphopeptide trapping for bovine α-casein. Mobile phase flow was delivered by a programmable syringe pump. *Mobile phase composition is shown in Table 2.

Step/fraction	Mobile phase	Flow rate (μl min^{-1})	Fraction-volume (μl)
Equilibration	LS*	20	Waste
FT	LS*	3	40
W1	LS*	20	40
W2	W2*	20	40
EL	ES*	4	40

Table 4
Nano-RPLC separation of tryptically digested α-casein. Mobile phases applied were MPA: 5% ACN, 0.1% FA; B: 15% ACN 15% MeOH, 0.1%FA; C: 60% ACN 30% MeOH 10% TFE, 0.08% FA.

	Minute	MPA (%)	MPB (%)	MFC (%)	Valve position
Sample loading	0–8	97	3	0	1_2
Gradient-1	8–45	0	100	0	6_1
Gradient-2	45–60	0	0	100	6_1
Wash	60–72	0	0	100	6_1
Equilibration	72–85	97	3	0	1_2

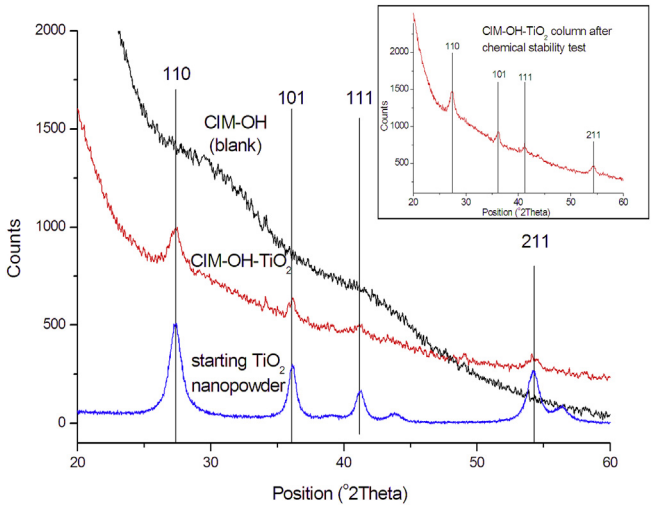

Fig. 1. XRD diffractograms of starting TiO_2 nanopowder, CIM-OH monolith and of CIM-OH-TiO_2 monolith before and after the chemical stability test.

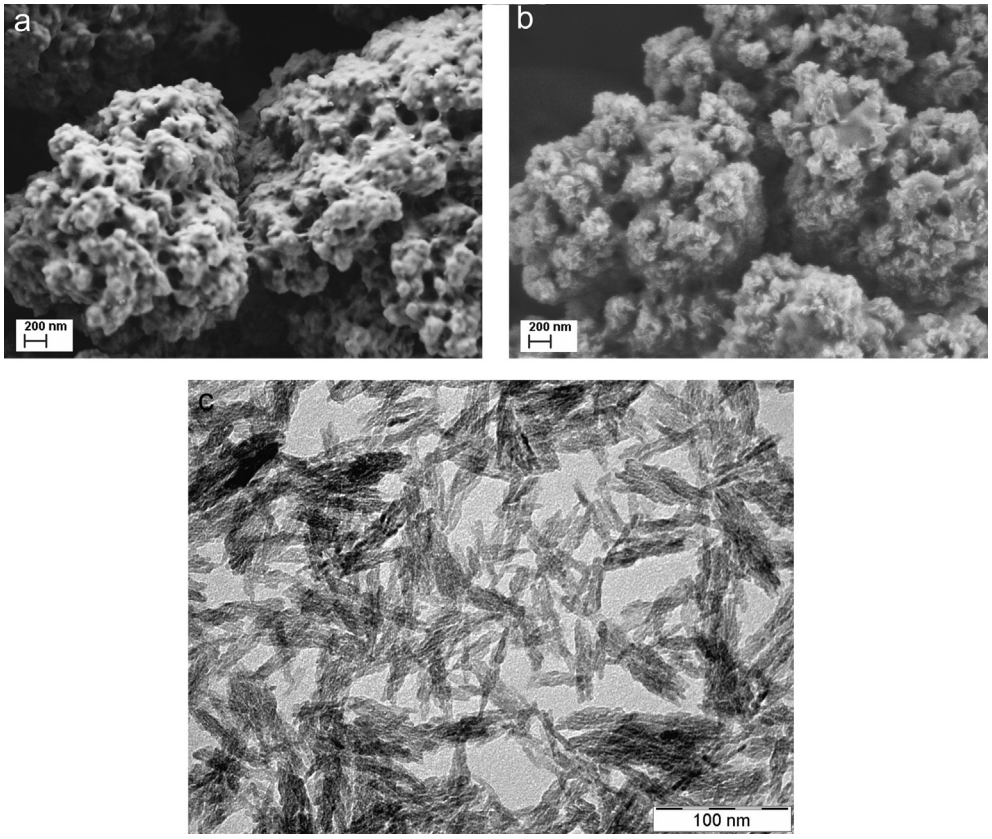

Fig. 2. SEM images of an CIM-OH monolith (A) on the left side and CIM-OH-TiO_2 monolith (B) on the right side. C) TEM image of TiO_2 nanoparticles. The TiO_2 nanoparticles are seen on the image B as needles on the surface of the monolith of approximately 100 nm lengths and 20 nm widths. The picture C is owned by University of Debrecen.

to an increase of the particle diameter beyond 100 nm. Monolith material with larger pore size distribution (with the average pore diameter 2.1 μm) was therefore used in subsequent studies, and no backpressure rise was observed.

The amount of immobilized TiO_2 was easily followed by turbidity measurements of the sol. Before loading onto the monolith, the suspension was turbid due to the presence of nanoparticles, but became transparent at the outlet of the monolith. The turbidity was monitored with absorbance at 600 nm. The estimated binding capacity for the TiO_2 nanoparticles was between 25 and 30 mg of TiO_2 per ml of column (data not shown) and more than 10 columns were prepared and used for subsequent experiments without facing any problems with TiO_2 loading repeatability. After reaching the dynamic binding capacity (DBC) for TiO_2, CIM-OH-TiO_2 columns were washed with 50 CV of dH_2O to remove any unbound nanoparticles. No elution of TiO_2 was noticed in this step. To verify that the binding of TiO_2 is not due to the physical entrapment within the monolith channels, the same immobilisation protocol was used using CIM epoxy columns with identical pore size as CIM-OH (2.1 μm). No binding of TiO_2 particles was observed to CIM-epoxy resin, and the turbidity of the sol at the outlet was identical (by visual inspection) as at the inlet.

The presence of a TiO_2 on a polymer surface and the morphology of the prepared composite were studied using a variety of physicochemical techniques. Initially, FTIR analysis of CIM-OH monoliths recorded in ATR mode was compared with the spectra of pure TiO_2 crystals, which were obtained after the evaporation of the solvent from the TiO_2 sol (Appendix, Fig. A.1). The FTIR spectrum of the CIM-OH monolith shows characteristic bands corresponding to O-H, C═O, C-H and C-O vibrations. The band with the strongest intensity at 1736 cm^{-1} corresponds to the ester carbonyl group from polymethacrylate backbone. The spectrum of TiO_2 standard contains two major broad bands at 3300 cm^{-1}, assigned to the O-H stretching vibration of Ti-OH groups, and 800 cm^{-1} assigned to the stretching mode of Ti-O-Ti [38]. The FTIR spectrum of the composite CIM-OH-TiO_2 material contains bands at same wavelengths as the CIM-OH with a decreased intensity of transmission at the wavenumbers, where main TiO_2 bands occur.

XRD diffractograms were then recorded to characterise the crystallinity of TiO_2 within the monolith composite (Fig. 1). Since TiO_2 used for the immobilisation was in rutile crystalline form, only the reflection peaks for rutile phase were expected.

The XRD diffractogram demonstrated that while there were no observed reflections for CIM-OH, there were four peaks arising from the baseline on the TiO_2 coated polymer – at 27.4, 36.1, 41.2 and 54.3°. These peaks correspond to the four most intense rutile peaks, (110 peak at 27.4°, 101 peak at 36.1, 211 peak at 54.3° and 111 peak at 41.2°), thus suggesting successful immobilisation of TiO_2 nanoparticles to the monolithic surface.

The morphology of CIM-OH-TiO_2 composite was studied with SEM, while TiO_2 particles were characterized by transmission electron microscopy (TEM). The images of CIM-OH (unmodified) and CIM-OH-TiO_2 (modified) monoliths are shown in Fig. 2A and B. While the surface of CIM-OH polymer globules is rounded and smooth, the surface of CIM-OH-TiO_2 is needle-shaped. The morphology of TiO_2 crystals used for immobilisation is needle-like of dimensions 100 nm × 10–20 nm (Fig. 2C). The size and the shape of needles, attached to the monolithic surface, match the morphology of TiO_2 particles recorded by TEM. No physical trapping of monolithic pores with TiO_2 is seen, but a homogeneous layer of TiO_2 with high homogenous coverage of the monolith surface by a layer of TiO_2 is observed by SEM.

In order to analyse the distribution of TiO_2 on the surface of the monolith support, pore size distribution analysis was performed with Hg porosimetry (Table 5). The average decrease in pore size diameter upon TiO_2 immobilisation is approximately 350 nm (Table 5), indicating that the thickness of the TiO_2 layer is approximately 175 nm. The layer thickness obtained from Hg porosimetry is larger than predicted from size of TiO_2 crystals, SEM images and from BET results analysis, but more importantly, no decrease of pore size distribution homogeneity was observed, and no additional pores with distinct pore sizes were identified with Hg porosimetry.

Based on the results of SEM studies, an increase in BET surface from non-modified to modified monolith was expected. The measurement of BET surface (Table 5) indicated an increase of surface area from 7.7 $m^2\ g^{-1}$ to 14.8 $m^2\ g^{-1}$. This difference is likely due to TiO_2 immobilisation, because measured BET surface area of dried starting TiO_2 material was 170 $m^2\ g^{-1}$. From the dynamic binding capacities for TiO_2, the BET surface area of immobilized TiO_2 needles would correspond to 13.8 m^2 TiO_2 per gram of the carrier, significantly higher than the value obtained from BET measurements (14.8−7.7 = 7.1 $m^2\ g^{-1}$). The difference between 7.1 and 13.8 $m^2\ g^{-1}$ could be rationalised assuming a decrease of exposed surface area due to the contact surface between the monolith and TiO_2 crystals. It is speculated that there is the highest probability of the adsorption of nanoparticles through their longer edges. Therefore the immobilisation results in a surface area decrease of two TiO_2 longer edges per one nanoparticle, what is approximatelly one half of the whole surface of TiO_2 rectangular structure. This is well in agreement with experimental results.

3.2. Stability of the CIM-OH-TiO_2 column

The stability of CIM-OH-TiO_2 monoliths was tested in 1.0 M NaOH, 0.1 M HCl and 96% ethanol solutions. In case of electrostatic adsorption of TiO_2 onto monolithic surface, desorption and/or precipitation of TiO_2 at strongly acidic or alkaline conditions should occur, while ethanol could affect CIM-OH-TiO_2 column and/or TiO_2-TiO_2 particles interaction, if hydrophobic forces are involved.

Columns are stable in pH range from 1 to 14 as well as in ethanol. No pressure problems were observed by pressure drop measurements on the pretreated columns. Additionally, CIM-OH-TiO_2 monoliths were characterized for TiO_2 presence after the application of the extreme chemical environment using FTIR, XRD and pore size distribution analyses. No statistical difference was observed (see XRD diffractogram – Fig. 1 - and pore size analyses – Table 5 - after the regeneration cycles), confirming strong interactions between OH functionality of the monolith and TiO_2 particles, and high chemical stability of the prepared composite material.

When the column is applied on-line, even an extremely small bleeding of nanoparticles could pose the damage of instruments parts behind the trap column. But because the TiO_2 nanoparticles are stable in solution as single particles only at very specific conditions, we expect fast aggregation of detached particle either with other desorbed particles (aggregated particle would be then trapped using on-line filters) or with TiO_2 particles immobilized on the column surface.

3.3. Simple chromatographic characterization of CIM-OH-TiO_2 monolith columns

In order to characterize the efficiency of phosphoprotein/phosphopeptide enrichment by CIM-OH-TiO_2, a chromatographic separation of model phosphoproteins (ovalbumin, beta casein, and phosvitin) was performed first, with the goal to separate them according to the density of phosphate groups. Ovalbumin contains two phosphorylation sites, beta casein up to five phosphorylation sites, and phosvitin up to 109 phosphate groups per one protein molecule [39]. As a negative control, cytochrome C, lysozyme, and human serum albumin were used as standards for nonphosphorylated proteins. Binding and eluting conditions were optimized and optimal binding was achieved by addition of 1% acetic acid or 0.1% TFA to the loading mobile phase. 100 mM NaCl was added to prevent nonspecific ionic interaction, while elution took place upon a change of pH value and increase of the phosphate concentration in the buffer (0.5 M sodium phosphate pH 12, data not shown). Due to a high nonspecific interaction of the negative control with CIM-OH-TiO_2 column even at low pH a separation of nonphosphorylated and phosphorylated proteins was not possible. In the elution step, elution of all proteins except phosvitin was observed, confirming that the latter binds to CIM-OH-TiO_2 tightly due to the presence of numerous phosphorylation sites. CIM-OH was therefore employed as an additional negative control to test for phosphoprotein separation. In the presence of 100 mM NaCl in 1% acetic acid, no binding of any studied proteins (ovalbumin, beta casein, and phosvitin as examples of phosphorylated proteins; cytochrome C, lysozyme and human serum albumin as examples of non-phosphorylated) to the CIM-OH column was observed, confirming that TiO_2 binds specifically to cytochrome C via non-defined interactions.

DBC was measured with a model phosphoprotein (ovalbumin) on CIM-OH-TiO_2 column and compared with the DBC measured for CIM-OH. The capacity measurements were performed in 1% acetic acid with 100 mM NaCl. The capacity is strongly dependent on buffer composition and its pH value. As expected, no adsorption of ovalbumin was observed on CIM-OH column. DBC of the CIM-OH-TiO_2 column was approximately 4.5 mg mL^{-1} of monolith (Fig. 3), thus suggesting the potential to use this chromatographic support for preparative chromatographic applications of phosphoprotein purification.

The breakthrough curve shows unusual increase of the signal between 0.4 and 0.6 min, what could be explained by different phosphorylation degree of ovalbumin, thus affecting its strength of interaction with the chromatographic support and consequently changing the dynamic binding capacity for different subspecies/isoforms of the same protein.

To further demonstrate the specificity of CIM-OH-TiO_2 for phosphoprotein enrichment, and to avoid the complex interaction of proteins with the stationary phase, the selectivity of the column was then tested for model phosphopeptide purification, performed under bind-elute conditions. Nonspecific binding of peptides to the TiO_2-immobilized monolith at low pH (0.1% TFA) was blocked with low concentration of salt (100 mM NaCl). Bound peptides were eluted in pH gradient 2–12 over 30 CV. Under conditions tested, no non-specific binding of nonphosphorylated peptide was observed

Table 5
BET analysis and pore size distribution of monoliths before and after the TiO_2 immobilisation. Additionally pore size distribution was measured after the application of the stability procedure and the results are gathered in the last column.

Sample	BET surface area ($m^2\ g^{-1}$ of dry monolith)	Average pore size diameter (nm)	Average pore size diameter after stability testing (nm)
CIM-OH column	7.7	1966	1940
CIM-OH-TiO_2 column	14.8	1590	1580
TiO_2 nanoparticles	170	Not measured	Not measured

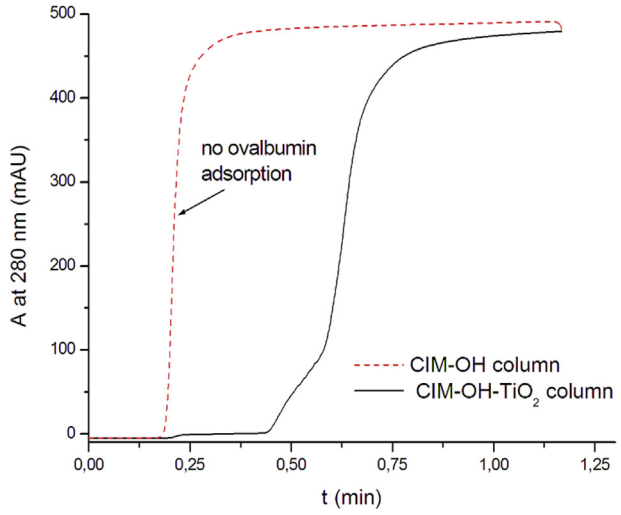

Fig. 3. DBC of ovalbumin (chicken egg albumin) CIM-OH and CIM-OH-TiO_2 columns. Binding buffer: 1% acetic acid +100 mM NaCl; flow rate 1.0 mL min^{-1}; ovalbumin concentration of 1 mg mL^{-1} in binding buffer.

on CIM-OH-TiO_2 column (peptide NP, Fig. 4left).

Peptides bearing phosphorylations at one or more residues were adsorbed to the support and were eluted in the pH gradient (Fig. 4left). A peak was observed in flow through fractions for all tested phosphopeptides (absorbance signal was measured at 280 and 215 nm, tryptophan fluorescence was also detected), prompting the question whether this corresponded incomplete adsorption of phosphopeptides, or to impurities in the peptide sample. The flow-through fraction was therefore collected and reapplied onto CIM-OH-TiO_2. Under bind-elute conditions, it did not bind to equilibrated CIM-OH-TiO_2 monolith (data not shown), suggesting that non-phosphorylated peptides and acidic peptides containing at least one tryptophan residue were present in all of the samples. The affinity of singly or multiply-phosphorylated peptides to CIM-OH-TiO_2 was similar; peptides eluted at approximately identical elution time, with some heterogeneity in peak distribution (two peaks: elution time 2.9 and 3.1 min). This was rationalised by the

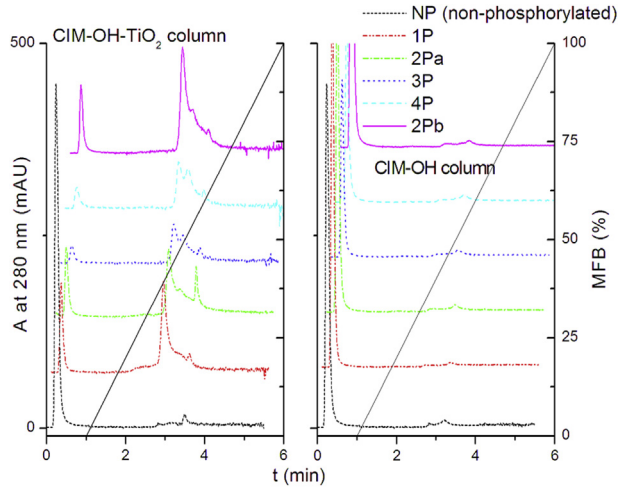

Fig. 4. The gradient elution of different phosphopeptides from CIM-OH-TiO_2 column (left) and CIM-OH column (right). The chromatographic conditions: binding buffer: 0.1% TFA, 100 mM NaCl, pH 2; MPB: 50 mM phosphate, pH 12; flow rate 1.0 mL min^{-1}; gradient from 0 to 100 MPB in 5 min, V_{inj} = 40 μL of peptide with concentration of 1.0 mg mL^{-1}.

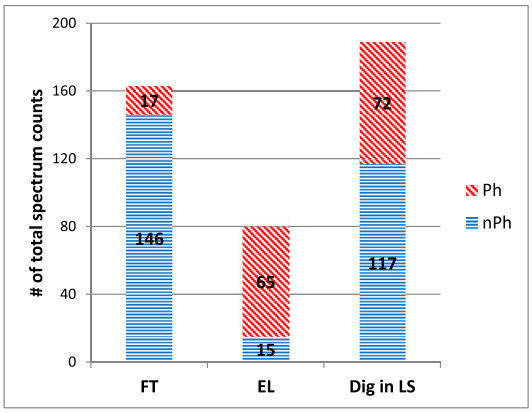

Fig. 5. MS identification rates of total phosphorylated (Ph) and non-phosphorylated (nPh) peptide counts derived from tryptically digested α1-and α2 bovine α-casein.

fact that the proximity of phosphorylation sites on the peptide chain prevented a correct positioning of the phosphate groups in a way that no more than one or two binding site with the CIM-OH-TiO_2 support was possible.

The experiments were then repeated using the CIM-OH column as a negative control. No adsorption was observed irrespective of the peptide sequence/modification pattern (Fig. 4right), suggesting that CIM-OH-TiO_2 chromatographic support has high affinity and specificity for binding for phosphopeptides. Treating CIM-OH-TiO_2 with 1.0 M NaOH, 0.1 M HCl or 20% ethanol, did not change its chromatographic parameters, suggesting high chemical stability of the column for regeneration and cleaning in place, and identifying it as robust chromatographic tool with high specificity for target biomolecules. The chromatographic experiments using selected peptides were performed on three technical replicates of CIM-OH-TiO_2 and three technical replicates of CIM-OH columns and no changes in selectivity for peptide binding were observed.

3.4. Phosphopeptide enrichment using tryptically digested bovine α-casein

Tryptically digested bovine α-casein was loaded on the micro-CIM-OH-TiO_2 column in order to assess binding ability of phosphopeptides and nonphosphorylated peptides from digested protein to the monolithic support. According to Fig. 5, most phosphopeptides carrying at least one phosphorylation residue were identified in the "EL" fraction, compared to peptides identified in the "FT" proving successful phosphopeptide trapping of the given column. The high extent of phosphopeptide identifications in the control sample "Dig in LS" reflects the successful depletion of phosphopeptides if compared to the FT.

Nevertheless, significant binding of non-phosphopeptides to the TiO_2 particles is present in the EL which contributes to suppression of MS identification of phosphopeptides. Further experiments should be conducted in order to improve phosphopeptide binding specificity and more important, the applicability of the column should be tested by performing phosphopeptide enrichment of tryptically digested complex biological samples.

4. Conclusions

We demonstrated a novel, simple and affordable procedure for the preparation of stable monolithic chromatographic columns with immobilized TiO_2 nanoparticles. The CIM-OH-TiO_2 columns were characterized using a variety of physical techniques, and the stability of TiO_2 layer was demonstrated under highly acidic, highly

alkaline or hydrophobic conditions.

Additionally, a simple chromatographic method based on ultraviolet and fluorescence detection for the qualification of prepared TiO_2 chromatographic supports was developed. Using the novel method with model peptides it was confirmed that CIM-OH-TiO_2 monolithic columns are capable of selective phosphopeptide separation.

It was demonstrated that a single-stage purification is sufficient for phosphopeptide enrichment, under low pH binding conditions, with a low concentration of salt (e.g. 100 mM NaCl), which prevents non-specific interactions of non-phosphorylated peptides with monolith surface. Peptides can be eluted using a shallow pH gradient, thereby offering a high resolution of the elution process. The phosphopeptide enrichment of digested bovine α-casein using micro-CIM-OH-TiO_2 chromatographic column has been additionally performed, showing a significant potential of novel column for enrichment of phosphopetides in proteomic studies. We, and others, are currently pursuing further work by demonstrating the applicability of the column for phosphopeptide enrichment for proteomic analyses of clinical biological materials.

Acknowledgements

We gratefully acknowledge dr. Zoltan Nagy and dr. Istvan Banyai from University of Debrecen, Hungary, for providing us TiO_2 nanoparticles and their TEM image; Darja Maučec from National Institute of Chemistry, Slovenia, is acknowledged for measuring the SEM images of the material. Miro Zdovc from Centre of excellence for biosensors, instrumentation and process control, Slovenia, is acknowledged for performing XRD measurements. We would like to thank dr. Rok Sekirnik for a gramatic review of the manuscript. Sandra Kontrec, Miroslava Legiša and Maša Velikonja from BIA Separations d.o.o. are acknowledged for their help in laboratory work.

Appendix A. Supplementary data

Supplementary data related to this article can be found at http://dx.doi.org/10.1016/j.aca.2016.08.044.

Funding sources

The Centre of Excellence for Biosensors, Instrumentation and Process Control (COBIK) is an operation financed by the European Union, European Regional Development Fund and Republic of Slovenia, Ministry of Education, Science, Culture and Sport. Support of this research by the European Union Seventh Framework Programme under grant agreement n° 282506 is also gratefully acknowledged. This work was financially supported in part by the Slovenian Research Agency within the research programme P4-0369.

References

[1] J.A. Ubersax, J.E. Ferrell Jr., Mechanisms of specificity in protein phosphorylation, Nat. Rev. Mol. Cell Biol. 8 (2007) 530–541.
[2] T. Pawson, J.D. Scott, Protein phosporylation in signaling - 50 Years and counting, Trends Biochem. Sci. 30 (2005) 286–290.
[3] U.K. Aryal, A.R. Ross, Enrichment and analysis of phosphopeptides under different experimental conditions using titanium dioxide affinity chromatography and mass spectrometry, Rapid Commun. Mass. Spectrom. 24 (2010) 219–231.
[4] C. Yang, X. Zhong, L. Li, Recent advances in enrichment and separation strategies for mass spectrometry-based phosphoproteomics, Electrophoresis 35 (2014) 3418–3429.
[5] H. Zhou, R. Tian, M. Ye, S. Xu, S. Feng, C. Pan, X. Jiang, X. Li, H. Zou, Highly specific enrichment of phosphopeptides by zirconium dioxide nanoparticles for phosphoproteome analysis, Electrophoresis 28 (2007) 2201–2215.
[6] E. Kanshin, S.W. Michnick, P. Thibault, Displacement of N/Q-rich peptides on TiO2 beads enhances the depth and coverage of yeast phosphoproteome analyses, J. Proteome Res. 12 (2013) 2905–2913.
[7] G. Gertler, G. Fleminger, H. Rapaport, Characterizing the adsorption of peptides to TiO2 in aqueous solutions by liquid chromatography, Langmuir 26 (2010) 6457–6463.
[8] G.T. Cantin, T.R. Shock, S.K. Park, H.D. Madhani, J.R. Yates, Optimizing TiO2-based phosphopeptide enrichment for automated multidimensional liquid chromatography coupled to tandem mass spectrometry, Anal. Chem. 79 (2007) 4666–4673.
[9] C.L. Nilsson, Advances in quantitative phosphoproteomics, Anal. Chem. 84 (2012) 735–746.
[10] T.E. Thingholm, O.N. Jensen, M.R. Larsen, Analytical strategies for phosphoproteomics, Proteomics 9 (2009) 1451–1468.
[11] A.N. Kettenbach, S.A. Gerber, Rapid and reproducible single-stage phosphopeptide enrichment of complex peptide mixtures: application to general and phosphotyrosine-specific phosphoproteomics experiments, Anal. Chem. 83 (2011) 7635–7644.
[12] L. Sang, Y. Zhao, C. Burda, TiO2 nanoparticles as functional building blocks, Chem. Rev. 114 (2014) 9283–9318.
[13] U. Cernigoj, U. Lavrencic Stangar, P. Trebse, Degradation of neonicotinoid insecticides by different advanced oxidation processes and studying the effect of ozone on TiO2 photocatalysis, Appl. Catal. B Environ. 75 (2007) 229–238.
[14] O. Carp, C.L. Huisman, A. Reller, Photoinduced reactivity of titanium dioxide, Prog. Solid State Chem. 32 (2004) 33–177.
[15] R. Sabertrasekh, H. Tiainen, S.P. Lyngstadaas, J. Reseland, H. Haugen, A novel ultra-porous titanium dioxide ceramic with excellent biocompatibility, J. Biomater. Appl. 25 (2011) 559–580.
[16] N.W. Duffy, K.D. Dobson, K.C. Gordon, B.H. Robinson, A.J. McQuillan, In-situ infrared spectroscopic analysis of the adsorption of ruthenium(II) bipyridyl dicarboxylic acid photosensitizers to TiO2 in aqueous solutions, Chem. Phys. Lett. 266 (1997) 451–455.
[17] A.D. Roddick-Lanzilotta, A.J. McQuillan, An in situ infrared spectroscopic study of glutamic acid and of aspartic acid adsorbed on TiO2: implications for the biocompatibility of titanium, J. Colloid Interface Sci. 227 (2000) 48–54.
[18] P.A. Connor, A.J. McQuillan, Phosphate adsorption onto TiO2 from aqueous Solutions: an in situ internal reflection infrared spectroscopic study, Langmuir 15 (1999) 2916–2921.
[19] S.R. Schmidt, F. Schweikart, M.E. Andersson, Current methods for phosphoprotein isolation and enrichment, J. Chromatogr. B 849 (2007) 154–162.
[20] Z. Lu, M. Ye, N. Li, W. Zhong, Y. Yin, Self-assembled TiO2 nanocrystal clusters for selective enrichmen, Angew. Chem. Int. Ed. 49 (2010) 1862–1866.
[21] J. Lu, C. Deng, X. Zhang, P. Yang, Synthesis of Fe3O4/graphene/TiO2 composites for the highly selective enrichment of phosphopeptides from biological samples, ACS Appl. Mater. Interfaces 5 (2013) 7330–7334.
[22] Y. Zhang, W. Ma, C. Zhang, C. Wang, H. Lu, Titania composite microspheres endowed with a size-exclusive effect toward the highly specific revelation of phosphopeptidome, ACS Appl. Mater. Interfaces 6 (2014) 6290–6299.
[23] S.T. Wang, M.Y. Wang, X. Su, B.F. Yuan, Y.Q. Feng, Organic-skinned inorganic nanoparticles: surface-confined polymerization of 6-(3-thienyl)hexanoic acid bound to nanocrystalline TiO2, Anal. Chem. 84 (2012) 7763–7770.
[24] A. Podgornik, S. Yamamoto, M. Peterka, N. Lendero Krajnc, Fast separation of large biomolecules using short monolithic columns, J. Chromatogr. B 927 (2013) 80–89.
[25] E. Mota, A. Sousa, U. Cernigoj, J.A. Queiroz, C.T. Tomaz, F. Sousa, Rapid quantification of supercoiled plasmid deoxyribonucleic acid using a monolithic ion exchanger, J. Chromatogr. A 1291 (2013) 114–121.
[26] D. Connolly, S. Currivan, B. Paull, Polymeric monolithic materials modified with nanoparticles for separation and detection of biomolecules: a review, Proteomics 12 (2012) 2904–2917.
[27] Y. Li, Y. Chen, R. Xiang, D. Ciuparu, L.D. Pfefferle, C. Horvath, J.A. Wilkins, Incorporation of single-wall carbon nanotubes into an organic polymer monolithic stationary phase for mu-HPLC and capillary electrochromatography, Anal. Chem. 77 (2005) 1398–1406.
[28] J. Krenkova, N.A. Lacher, F. Svec, Control of selectivity via nanochemistry: monolithic capillary column containing hydroxyapatite nanoparticles for separation of proteins and enrichment of phosphopeptides, Anal. Chem. 82 (2010) 8335–8341.
[29] S.D. Chambers, T.W. Holcombe, F. Svec, J.M. Frechet, Porous polymer monoliths functionalized through copolymerization of a C60 fullerene-containing methacrylate monomer for highly efficient separations of small molecules, Anal. Chem. 83 (2011) 9478–9484.
[30] J. Krenkova, F. Foret, Iron oxide nanoparticle coating of organic polymer-based monolithic columns for phosphopeptide enrichment, J. Sep. Sci. 34 (2011) 2106–2112.
[31] D. Connolly, B. Twamley, B. Paull, High-capacity gold nanoparticle functionalised polymer monoliths, Chem. Commun. 46 (2010) 2109–2111.
[32] P.Z. Araujo, P.J. Morando, M.A. Blesa, Interaction of catechol and gallic acid with titanium dioxide in aqueous suspensions. 1. Equilibrium studies, Langmuir 21 (2005) 3470–3474.
[33] G. Giorgi, J.I. Fujisaw, H. Segawa, K. Yamashita, Unraveling the adsorption mechanism of aromatic and aliphatic diols on the TiO2 surface: a density functional theory analysis, Phys. Chem. Chem. Phys. 15 (2013) 9761–9767.
[34] M. Mazanek, E. Roitinger, O. Hudecz, J.R. Hutchins, B. Hegemann, G. Mitulovic, T. Taus, C. Stingl, J.M. Peters, K. Mechtler, A new acid mix enhances phosphopeptide enrichment on titanium- and zirconium dioxide for mapping of

phosphorylation sites on protein complexes, J. Chromatogr. B Anal. Technol. Biomed. Life Sci. 878 (2010) 515–524.
[35] M. Mazanek, G. Mitulovic, F. Herzog, C. Stingl, J.R. Hutchins, J.M. Peters, K. Mechtler, Titanium dioxide as a chemo-affinity solid phase in offline phosphopeptide chromatography prior to HPLC-MS/MS analysis, Nat. Protoc. 2 (2007) 1059–1069.
[36] G. Mitulovic, C. Stingl, I. Steinmacher, O. Hudecz, J.R. Hutchins, J.M. Peters, K. Mechtler, Preventing carryover of peptides and proteins in nano LC-MS separations, Anal. Chem. 81 (2009) 5955–5960.
[37] P. Bardou, J. Mariette, F. Escudie, C. Djemiel, C. Klopp, Jvenn: an interactive venn diagram viewer, BMC Bioinforma. 15 (2014) 293–299.
[38] M. Tasbihi, U. Lavrencic Stangar, U. Cernigoj, J. Jirkovsky, S. Bakardjieva, N. Novak Tusar, Photocatalytic oxidation of gaseous toluene on titania/mesoporous silica powders in a fluidized-bed reactor, Catal. Today 161 (2011) 181–188.
[39] UniProt Home Page. http://www.uniprot.org/uniprot/(accessed 02.03.15).